National Center for Theoretical Sciences

Continuum Gating Current Models Computed with Consistent Interactions

Tzyy-Leng Horng
Robert S. Eisenberg
Chun Liu
Francisco Bezanilla

NCTS/Math
Technical Report
2018-020

Continuum Gating Current Models Computed with Consistent Interactions

Tzyy-Leng Horng[1,5], Robert S. Eisenberg[2], Chun Liu[3], Francisco Bezanilla[4]

[1]Department of Applied Mathematics, Feng Chia University, Taichung, Taiwan 40724

[2] Department of Applied Mathematics, Illinois Institute of Technology, Chicago, Illinois, 60616, United States

Department of Physiology and Biophysics, Rush University, Chicago, Illinois 60612, United States

[3]Department of Mathematics, Pennsylvania State University, University Park, Pennsylvania 16802, United States

[4]Department of Biochemistry and Molecular Biology and Institute for Biophysical Dynamics, University of Chicago, Chicago, Illinois 60637, United States

[5]National Center for Theoretical Sciences, National Taiwan University, Taipei, Taiwan 106

ABSTRACT

The action potential of nerve and muscle is produced by voltage sensitive channels that include a specialized device to sense voltage. The voltage sensor depends on the movement of charges in the changing electric field, as suggested by Hodgkin and Huxley. Gating currents of the voltage sensor are now known to depend on the movements of positively charged arginines through the hydrophobic plug of a voltage sensor domain. Transient movements of these permanently charged arginines, caused by the change of transmembrane potential **V**, further drag the S4 segment and induce opening/closing of ion conduction pore by moving the S4-S5 linker. This moving permanent charge induces capacitive current flow everywhere. Everything interacts with everything else in the voltage sensor and protein so it must also happen in its mathematical model. A PNP-steric model of arginines and a mechanical model for the S4 segment are combined using energy variational methods in which all densities and movements of charge satisfy conservation laws, which are expressed as partial differential equations in space and time. The model computes gating current flowing in the baths produced by arginines moving in the voltage sensor. The model also captures the capacitive pile up of ions in the vestibules that link the bulk solution to the hydrophobic plug. Our model reproduces signature properties of gating current: (1) equality of ON and OFF charge Q in integrals of gating current (2) saturating voltage dependence in QV curve and (3) many (but not all) details of the shape of gating current as a function of voltage. Our results agree qualitatively with experiments, and can be improved by adding more details of the structure and its correlated movements. The proposed continuum model is a promising tool to explore the dynamics and mechanism of the voltage sensor.

Keywords: ion channel; voltage sensor; gating current; arginine; S4; PNP-steric model

INTRODUCTION

Much of biology depends on the voltage across cell membranes. The voltage across the membrane must be sensed before it can be used by proteins Permanent charges[1] move in the strong electric fields within membranes, so carriers of sensing charge were proposed as voltage sensors even before membrane proteins were known to span lipid membranes [1]. Movement of permanent charges of the voltage sensor is gating current and movement is the voltage sensing mechanism.

Knowledge of membrane protein structure has allowed us to identify and look at the atoms that make up the voltage sensor. Protein structures do not include the membrane potentials and macroscopic concentrations that power gating currents, and therefore simulations are needed. Atomic level simulations like molecular dynamics do not provide an easy extension from the atomic time scale $\sim 10^{-15}$ sec to the biological time scale of gating currents that starts at $\sim 10^{-6}$ sec and reaches $\sim 10^{-2}$ sec. Calculations of gating currents from simulations must average the trajectories (lasting $\sim 10^{-1}$ sec sampled every 10^{-15} sec) of $\sim 10^{6}$ atoms all of which interact through the electric field to conserve charge and current, while conserving mass. It is difficult to enforce continuity of current flow in simulations of atomic dynamics because simulations compute only local behavior while continuity of current is global, involving current flow far from the atoms that control the local behavior. It is impossible to enforce continuity of current flow in calculations that assume equilibrium (zero net flow) under all conditions.

A hybrid approach is needed, starting with the essential knowledge of structure, but computing only those parts of the structure used by biology to sense voltage. In close packed ('condensed') systems like the voltage sensor, or ionic solutions, '*everything interacts with everything else*' because electric fields are long ranged as well as exceedingly strong [2]. In ionic solutions, ion channels, even in enzyme active sites, steric interactions that prevent the overfilling of space in well-defined protein structures are also of great importance as they produce short range correlations [3].

Closely packed charged systems are well handled mathematically by energy variational methods. Energy variational methods guarantee that all variables satisfy all equations (and boundary conditions) at all times and under all conditions and are thus always consistent. We use the energy variational approach developed in [4] and [5] to derive a consistent model of gating charge movement, based on the basic features of

[1] Permanent charge is our name for a charge or charge density independent of the local electric field, for example, the charge and charge distribution of Na^+ but not the charge in an highly polarizable anion like Br^- or the nonuniform charge distribution of H_2O in the liquid state with its complex time dependent (and perhaps nonlinear) polarization response to the local electric field.

the structure of crystallized voltage sensitive channels. A schematic of the model is shown below. The continuum model we use simulates the mechanical dynamics in a single voltage sensor, while the experimental data is from many independent voltage sensors. Ensemble averages of independent voltage sensors recording is equivalent to macroscopic continuum modeling in a single voltage sensor, if correlations are captured correctly in the model of the single voltage sensor.

THEORY: MATHEMATICAL MODEL

The reduced mechanical model for a voltage sensor is shown in Fig. 1(a) with four arginines R_i, i=1, 2, 3, 4, each attached to the S4 helix by identical springs with the same spring constant K. The electric field will drag these four arginines since each arginine carries +1 charge. The charged arginines can also move as a group. S4 connect to S3 and S5 at its two ends by identical springs with spring constant $K_{S4}/2$.

Once the membrane is depolarized from say −90mV inside negative, to +10mV inside positive, arginines together with S4 will be driven towards the extracellular side. A repolarization from +10mV volts to −90mV, move the arginines back to the intracellular side. This movement is the basic voltage sensing mechanism. The movement of S4 triggers the opening or closing of the lower gate—consisting mainly of S6 forming the ion permeation channel—by a mechanism widely assumed to be mechanical, although electrical aspects of the linker motion are likely to be involved, as well.

When arginines are driven by electric field, they are forced to move through a hydrophobic plug, composed by several nonpolar amino acids from S1, S2 and S3 [6]. Arginines reside initially in the hydrated lumen of the intracellular vestibule. They then move though the hydrophobic plug, and wind up in the vestibule on extracellular side. This movement involves dehydration when the arginines move through the hydrophobic plug, where the arginines encounter a barrier in the potential of mean force (PMF) mainly dominated by the difference of the solvation energy in bulk situation and in the hydrophobic plug [7]. Note that Na^+ and Cl^- (which are the only ions in the bulk solution in this paper, for simplicity) are found only in vestibules and are not allowed into the hydrophobic plug in our model. The ends of the two vestibules on each side of the system act as impermeable walls for Na^+ and Cl^- in our model. When the voltage is turned on and off, these two walls store/release charge (carried by ions) in their electric double layers (EDL) that have many of the properties of capacitors.

In the present continuum model, the four arginines R_i, i=1, 2, 3, 4, are described by their individual density distributions (concentrations) c_i, i=1, 2, 3, 4, allowing the arginines to interact with Na^+ and Cl^- in vestibules. The density (i.e., concentration)

distributions represent probability density functions as shown explicitly in the theory of stochastic processes, used to derive such equations in [8] using the general methods of [9]. The important issue here is how well the correlations are captured in the continuum model. Some are more likely to be faithfully captured in molecular dynamics simulations (e.g., more or less local hard sphere interactions), others in continuum models (e.g., correlations induced by far field boundary conditions like the potentials imposed by bath electrodes to maintain a voltage clamp).

Here we treat the S4 itself as a rigid body so we can capture the basic mechanism of a voltage sensor without considering the full details of structure, which might lead to a three dimensional model difficult to compute in reasonable time. We construct an axisymmetric 1D model with a three-zone geometric configuration illustrated in Fig. 1(b) following Fig. 1(a). Zone 1 with $z \in [0, L_R]$ is the intracellular vestibule; zone 2 with $z \in [L_R, L_R + L]$ is the hydrophobic plug; zone 3 with $z \in [L_R + L, 2L_R + L]$ is the extracellular vestibule. Arginines, Na^+, and Cl^- can all reside in zone 1 and 3. Zone 2 only allows the residence of arginines, albeit with a severe hydrophobic penalty because of their permanent charge, in a region of low dielectric coefficient hence called hydrophobic.

Based on Fig. 1(b), the governing 1D dimensionless PNP-steric equations are expressed below with the detailed non-dimensionalization process shown in Section 1 of supplementary information. The first one is Poisson equation that shows how charge creates potential:

$$-\frac{1}{A}\frac{d}{dz}\left(\Gamma A \frac{d\phi}{dz}\right) = \sum_{i=1}^{N} z_i c_i , \qquad i = \mathrm{Na}, \mathrm{Cl}, 1, 2, 3, 4, \tag{1}$$

with $z_{Na} = 1$, $z_{Cl} = -1$, $z_i = z_{arg} = 1, i = 1, 2, 3, 4$, $\Gamma = \frac{\lambda_D^2}{R^2}$ and $A(z)$ being the cross-sectional area. For zones 1 and 3, $\Gamma = 1$ since here the arginines are fully hydrated with $\varepsilon_r = 80$. For zone 2, we assume a hydrophobic environment with $\varepsilon_r = 8$, and therefore $\Gamma = 0.1$. Dielectric constant inside the hydrophobic plug (zone 2) is not experimentally available, however the computational result is not sensitive to this value based on our sensitivity analysis.

The second equation is the species transport equation based on conservation laws:

$$\frac{\partial c_i}{\partial t} + \frac{1}{A}\frac{\partial}{\partial z}(AJ_i) = 0, \qquad i = \mathrm{Na}, \mathrm{Cl}, 1, 2, 3, 4. \tag{2}$$

with the content of J_i expressed below based on Nernst-Planck equation for Na^+ and Cl^-:

$$J_i = -D_i\left(\frac{\partial c_i}{\partial z} + c_i z_i \frac{\partial \phi}{\partial z}\right), \quad i = \mathrm{Na}, \mathrm{Cl}, \quad z \text{ in zone 1 and 3}, \tag{3}$$

and for 4 arginines c_i, i=1, 2, 3 and 4, based on Nernst-Planck equation with steric effect and some imposed potentials:

$$J_i = -D_i\left(\frac{\partial C_i}{\partial z} + z_{arg}C_i\frac{\partial \phi}{\partial z} + C_i\left(\frac{\partial V_i}{\partial z} + \frac{\partial V_b}{\partial z}\right) + gC_i\sum_{j\neq i}\frac{\partial C_j}{\partial z}\right),\ z\ in\ \text{all zones},\quad (4)$$

The first and second terms in Eqs. (3,4) describe diffusion and electro-migration respectively. The third terms in Eq. (4) are external potential terms with V_i, i=1, 2, 3 and 4 being the constraint potential for the 4 arginines c_i to S4, represented here by a spring connecting each arginine c_i to S4, as shown in Fig. 1(a). Governing equations Eqs. (1-4) were derived by energy variational methods, that is further shown in Section 3 of supplementary information.

The elastic system is described by

$$V_i(z,t) = K(z - (z_i + Z_{S4}(t)))^2, \quad (5)$$

where K is the spring constant, z_i is the fixed anchoring position of the spring for each arginine c_i on S4, $Z_{S4}(t)$ is the center-of-mass z position of S4 by treating S4 as a rigid body. Here, we set z_1=0.6, z_2=0.2, z_3=-0.2, z_4=-0.6 using structural information that gives the arginine anchoring interval on S4 as 0.4nm. $Z_{S4}(t)$ follows the motion of equation based on spring-mass system:

$$m_{S4}\frac{d^2Z_{S4}}{dt^2} + b_{S4}\frac{dZ_{S4}}{dt} + K_{S4}(Z_{S4} - Z_{S4,0}) = \sum_{i=1}^{4} K\left(z_{i,CM} - (z_i + Z_{S4})\right), \quad (6)$$

where m_{S4}, b_{S4} and K_{S4} are the mass, damping coefficient and restraining spring constants for S4. $Z_{S4,0}$ is the natural (i.e., 'resting') position of $Z_{S4}(t)$. Here, $z_{i,CM}$ is the center of mass for the set of arginines c_i , which can be calculated by

$$z_{i,CM} = \frac{\int_0^{L+2LR} A(z)zc_i dz}{\int_0^{L+2LR} A(z)c_i dz}, \quad i=1, 2, 3, 4. \quad (7)$$

We assume that the spring mass system for S4 is over-damped, which means the inertia term in Eq. (6) can be neglected.

The energy barrier V_b in Eq. (4) is nonzero only in zone 2, which mainly represents the difference in solvation energy, chiefly characterized by difference of dielectric constants, in the hydrophobic plug and bulk solution. The structure of the energy barrier is actually very complicated. Here, we simply assume a hump shape for PMF (see more in Section 2 of supplementary information), although we will seek greater realism in later work.

The last term in Eq. (4) is the steric term that accounts for steric interaction among arginines [5,10]. Here we set g=0.5, a reasonable value. Though there is actually no experimental measurement available for g, the computation results have been verified to be insensitive to its value.

Here we assume quasi-steady state for Na^+ and Cl^-, which means $\frac{\partial c_i}{\partial t} = 0, i = Na, \mathrm{Cl},$ in Eq. (2), and the reason is elaborated in Section 4 of supplementary information. The formulation of boundary and interface conditions is also shown in Section 5 of supplementary information.

Besides the main input parameter V, which is the applied voltage bias (corresponding to the command potential in voltage clamp experiments), other parameters like D_i, i=1, 2, 3, 4, K, K_{S4}, b_{S4} are also required. Results are especially sensitive to the values of K, K_{S4}, b_{S4}. We have tried and found D_i=50, i=1,2,3,4, K=3, K_{S4}=3, b_{S4}=1.5 provide the best fit to the important experiments reported in [11]. Some additional explanation on fitting these parameter values is referred to Section 6 of supplementary information.

Usually the electric current in the ion channel is treated simply as the flux of charge and is uniform in the z direction when steady in time. This is not so in the present non-steady dynamic situation, since storing and releasing of charge in vestibules are involved. Here, the flux of charge at the middle of hydrophobic plug, z= L_R+L/2, was computed to estimate the experimentally observed gating current. However, it is actually impossible (so far) to experimentally measure the current at the middle of hydrophobic plug. In experiments, the voltage clamp technique is used, and on/off gating current through the membrane is measured, which should be equal to the flux of charge at z=0 in the present frame work as shown in Fig. 1(b). The flux of charges at any z position $I(z,t)$ can be related to the flux of charges at z=0, $I(0,t)$, simply by charge conservation:

$$\frac{\partial}{\partial t} Q_{net}(z,t) = I(0,t) - I(z,t), \tag{8}$$

where

$$Q_{net}(z,t) = \int_0^z A(\xi) \sum_{all\ i} z_i c_i d\xi, \tag{9}$$

and flux of charges at any z position $I(z,t)$ is defined by

$$I(z,t) = A(z) \sum_{all\ i} z_i J_i(z,t). \tag{10}$$

We identify $\frac{\partial}{\partial t} Q_{net}(z,t)$ as the displacement current, and denote it as $I_{disp}(z,t)$, since Eq. (7) is equivalent to Ampere's law in Maxwell's equations, and $\frac{\partial}{\partial t} Q_{net}(z,t)$ is exactly the displacement current in Ampere's law. The proof is elaborated in Section 7 of supplementary information. A general discussion about displacement current can be found in [12-14] that does not involve assumptions concerning the

dielectric coefficient ε_r or polarization properties of matter at all. Hence, Eq. (8) can be simply re-written as

$$I_{tot}(z,t) = I(z,t) + I_{disp}(z,t) = I(0,t), \quad (11)$$

where we define the sum of displacement current and flux of charges as the total current $I_{tot}(z,t)$. The z-distribution of the total current should be uniform by Kirchhoff's law, and we verify this by computations shown in the section under heading *Flux of charges at different locations*.

We are also interested in observing the net charge at vestibules. Consider, for example, the net charge at the intracellular vestibule, $Q_{net}(L_R,t)$. The net charge consists of arginine charges and their counter charges formed by the EDL of ionic solution in that location. Electro-neutrality is approximate but will not be exact there. Flux of charge, displacement current and net charge at vestibules will be discussed further in the section under heading *Flux of charges at different locations*.

To evaluate the current theoretical model, it is important to compare our computational results with experimental measurements [11] in the curves of gating current and amount of gating charge moved versus applied voltage (IV and QV curves). To construct the QV curve, we calculate $Q_1 = \int_0^{L_R} A(z)\sum_{i=1}^4 c_i dz$, $Q_2 = \int_{L_R}^{L_R+L} A(z)\sum_{i=1}^4 c_i dz$, $Q_3 = \int_{L_R+L}^{2L_R+L} A(z)\sum_{i=1}^4 c_i dz$, which are the amounts of arginine found in zone 1, 2 and 3, respectively. Usually $Q_2 \approx 0$ is due to the energy barrier V_b in zone 2. Arginines tend to jump across zone 2 when driven from zone 1 to zone 3 as the voltage V is turned on. The number of arginines that move and settles at zone 3 depends on the magnitude of V. Besides IV and QV curves, the time course of the movement of arginines and S4, $z_{i,CM}(t)$ and $Z_{S4}(t)$, is important to report here, since recording these movements in experiments becomes feasible nowadays by optical methods. Many qualitative models accounting for the movement of S4 and conformation change of the voltage sensor have been proposed. Readers are referred to review papers [15,16] for more details.

Eqs. (1-4) are first discretized in space by high-order multi-block Chebyshev pseudospectral methods, and then integrated in time under the framework of method of lines. Details of numerical method is referred to Section 8 of supplementary information.

RESULTS AND DISCUSSION

Here numerical results based on the mathematical model described above were calculated and compared with experimental measurements [11]. Our 1D continuum

model has advantages and disadvantages. The lack of 3D structural detail means that some details of the gating current and charge cannot be reproduced. It should be noted however that to reproduce those, one needs more than just static structural detail. One must also know how the structures (particularly their permanent and polarization charge) change after a command potential is applied, in the experimental ionic conditions. The 1D model has advantages because it computes the actual experimental results on the actual experimental time scale, in realistic ionic solutions and with far field boundary conditions actually used in voltage clamp experiments. It also conserves current as we will demonstrate later. Conservation of current needs to be present and verified in theories and simulations since it is a universal property of the Maxwell equations [12-14].

QV curve

When the membrane and voltage sensor is held at a large inside negative potential (e.g., hyperpolarized to -90mV), S4 is in a resting position and all arginines stay in the intracellular vestibule. When the potential is made more positive (e.g., depolarized to +10mV), S4 is in the active position and all arginines are at the extracellular vestibule.

The voltage dependence of the charge (arginines) transferred from intracellular vestibule to extracellular vestibule is characterized as a QV curve in experimental papers and it is sigmoidal in shape [11]. Fig. 2(a) shows that our computed QV curve— the dependence of Q_3 on V—is in very good agreement with the experiment [11]. This good agreement comes from the facts that our resultant QV curve is also a sigmoidal curve, and, most important of all, the slope of QV curve can be tuned, mainly by the adjustment of K, K_{S4}, b_{S4}, to agree with experiment. Rare theoretical models can achieve this agreement especially for the slope. An example of mismatch was reported in [17,18]. Fig. 2(b) shows the steady-state distributions of Na^+, Cl^- and arginines in the inside negative, hyperpolarized situation (V=-90mV). As we can see, all the arginines stay in the intracellular vestibule, and none of the arginines moves to the extracellular vestibule ($Q_3 \approx 0$).

Fig. 2(c) shows the situation at V=-48mV, which is the midpoint of the QV curve. As we can see, each vestibule has distributions of c_i, i=1,2,3,4, resulting in half of the arginines staying in it ($Q_3 = 2$). Judging from the center-of-mass position for each arginine, as shown later in Fig. 6, it can be deduced that R1 and R2 are in the extracellular vestibule, and R3 and R4 are in the intracellular vestibule. There are almost no arginines in zone 2 (hydrophobic plug) due to the energy barrier in it. Note that this represents an average because in a single molecule interpretation, half of the sensors will be with all R's inside and the other half with all R's outside. The

midpoint of -48 mV from [11] requires the natural position of S4, $Z_{S4,0}$, to be biased from $L_R + 0.5L$ to $Z_{S4,0} = L_R + 0.5L + 1.591$nm, otherwise the midpoint would be 0 mV. Fig. 2(d) shows the situation at full depolarization (*V*=-8mV), where all arginines move to extracellular vestibule ($Q_3 \approx 4$) in the fully depolarized, activated state.

Gating current

Fig. 3 shows the time course of gating currents, observed as flux of charge at the middle of hydrophobic plug $I(L_R + L/2, t)$, due to the movement of arginines when the membrane is largely depolarized, and partially depolarized. In the case of large depolarization, *V* rises from -90mV at *t*=10 to -8mV, and drops back to -90mV at *t*=150 (Fig. 3(a)). Time course of gating current and contributions of individual arginines are shown in Fig. 3(b). As expected, the rising order of each current component follows the moving order of R1, R2, R3 and R4 when depolarized, and that order is reversed when repolarized. The area under the gating current is the amount of charge moved. Since arginines move forward and backward in this depolarization/repolarization scenario, the areas under the ON current and the OFF current are same. The areas are equal for each component of current as well. The equality of area is an important signature of gating current that contrasts markedly with the properties of ionic current [19,20]. In the case of partial depolarization (*V* rises from -90mV to -50mV at *t*=10 to and drops back to -90mV at *t*=150, Fig. 3(c)), the time course of gating current and its four components contributed by each arginine for this situation is shown in Fig. 3(d). Under this partial polarization, not all arginines move past the middle of hydrophobic plug due to weaker driving force in partial polarizations compared with large depolarization case and this can be observed from the areas under each component current being different (Fig. 3(d)).

The gating currents can be better understood by looking at a sequence of snapshots showing the spatial distribution of electric potential, species concentration and electric current. The distributions at several times are shown in Fig. 4(a) for the case of sudden change in command voltage to a more positive value, a large depolarization, and Fig. 4(b) for the case of a partial depolarization. The electric potential profiles at *t*=13 and *t*=148 show that the profile of electric potential changes as arginines move from left to right even though the voltage is maintained constant across the sensor. As highlighted by those equipotential lines superposed on the graph of voltage sensor domain in Fig. 4, this is not a constant field system at all [21]! Slight bulges in electric potential profile exist wherever arginines are dense. This can be easily explained by understanding the effect of Eq. (1) on a concave spatial distribution of electric potential.

In Fig. 4, total current defined in Eq. (11), though changing with time, is always constant in *z* at all times, satisfying Kirchhoff's law, i.e., conservation of current. At *t*=13, when gating current is substantial (Fig. 3b and 3d), we can visualize the *z*-distributions of flux of charges $I(z,t)$, displacement of current $I_{disp}(z,t)$ and total current $I_{tot}(z,t)$ individually in Fig. 4.

Flux of charges at different locations

Flux of charges $I(z,t)$, together with displacement current $I_{disp}(z,t)$ and total current $I_{tot}(z,t)$, depicted in Fig. 4, deserves more discussion here. Though $I(z,t)$, $I_{disp}(z,t)$ and $I_{tot}(z,t)$ are well defined in Eqs. (8-11), the actual computation of them takes an indirect ~~way~~ path due to the assumption of quasi-steady state for Na^+ and Cl^- in Eq. (2). The details are referred to Section 9 of supplementary information. The computed total current $I_{tot}(z,t)$ does indeed ~~uphold~~ satisfy Kirchhoff's law by its uniformity in *z*. This verification is shown in Fig. 4 at several times, and we have checked that is in fact true at any time.

In the bottom rows of Fig. 4 at *t*=13, we observe that $I(z,t)$ is generally non-uniform in *z* and is accompanied by congestion/decongestion of arginines in between. However $I(z,t)$ is almost uniform at zone 2 (hydrophobic plug), which means almost no congestion/decongestion of arginines occurs there, and therefore no contribution to the displacement current $\frac{d}{dt}Q_{net}(z,t)$ from zone 2. This is because arginines can hardly reside at zone 2 due to the energy barrier in it.

Several things are worth noting in the time courses of $I\left(L_R+\frac{L}{2},t\right)$, and $I(0,t)$ (equal to uniformly distributed I_{tot} as depicted by Eq. (11)) illustrated in Fig. 5(a) under the case of large depolarization. First, $I\left(L_R+\frac{L}{2},t\right)$ is noticeably larger than $I(0,t)$ in the ON period. This is because their difference, exactly the displacement current I_{disp}, is always negative at zone 2 when depolarized, since arginines are leaving zone 1 and make $\frac{d}{dt}Q_{net}<0$ for zone 2. It is expected the area under the time course of $I\left(L_R+\frac{L}{2},t\right)$ would be very close to 4e, as verified by the time courses of Q_3 in Fig. 5(b). We use $I(0,t)$ to estimate the experimentally measured voltage-clamp current while the counterpart area of experimentally measurable $I(0,t)$ would be less than 4e due to its smaller magnitude compared with $I\left(L_R+\frac{L}{2},t\right)$. This may partly explain the experimental observations that at most 13e

[16,22,23], instead of 16e, are moved during full depolarization in 4 voltage sensors (for a single ion channel) based on computing the area under voltage-clamp gating current. Therefore, flux of charge at any location of zone 2, though impossible to measure in experiments so far, will give us amount of arginines moved during depolarization more reliably than the measurable $I(0,t)$.

Second, we see in Fig. 5(a) with magnification in its inset plot that, as in experiments, $I(0,t)$, but not $I\left(L_R+\frac{L}{2},t\right)$, has contaminating leading spikes in ON and OFF parts of the current. These spikes are capacitive currents from solution EDL of vestibules caused by sudden rising and dropping of command potential. These spikes need to be removed in voltage-clamp experiments in order to get rid of the contribution from solution EDL (and membrane) to the transport of gating charges (arginines) when computing the area under gating current. The technical details of removing these spikes are shown in Section 10 of supplementary information, and more details about spikes can be found in Section 11 of supplementary information.

Third, in Fig. 5(b), as arginines move from one vestibule to another, the concentrations of Na^+ and Cl^- also correspondingly change with time at the vestibules. They form counter charges through EDL, and balance arginine charges at vestibules. However, these EDL changes only maintain approximate, not exact, charge balance as shown in Fig. 5(b). The violation of electroneutrality causes the displacement current, that is not negligible.

As in the previous section, we used flux of charges at the middle of hydrophobic plug, $I(L_R+L/2\,,t)$, instead of experimentally measurable $I(0,t)$ to represent the gating current in discussions. We may as well name $I(L_R+L/2\,,t)$ as arginine current in order to avoid the confusion with the actual gating current $I(0,t)$ here. This arginine current leaves out its associated displacement current $I_{disp}(L_R+L/2\,,t)$, and serves to represent gating current better for two reasons:

(1) The area under time course of $I(L_R+L/2\,,t)$ gives us the amount of arginines moved during depolarization more faithfully than $I(0,t)$. The fluxes of charge for each arginine shown in Fig. 3(b) and Fig. 3(d) carry important information about how each arginine is moved by the electric field, that will be further illustrated in Fig. 6. All these will not be easy to display and comprehend if we use $I(0,t)$ instead.

(2) Using $I(0,t)$ as a definition of gating current would require a decontamination by removing the leading spikes ~~in it~~, which is computationally costly. Especially, ~~it~~ removing spikes would pose a heavy numerical burden

when doing parameter fitting, where numerous repeated computations need to be conducted.

Time course of arginine and S4 translocation

Fig. 6 shows the time course of Q (amount of arginines moved to extracellular vestibule, equal to Q_3 here) and center-of-mass trajectories of individual arginines ($z_{i,CM}$, i=1, 2, 3, 4) and S4 segment (Z_{S4}). Figs. 6(a) and 6(b) show the case of large depolarization and Figs. 6c and 6d show the case of smaller, partial depolarization.

In the case of large depolarization (Fig. 6(b)) the arginines and S4 z-positions quickly reach individual steady states with almost all arginines transferred to the extracellular vestibule, as previously shown in Fig. 4(a). Therefore, Q is close to its saturated value 4, as shown in Fig. 6(a). Arginines and S4 move back to the intracellular vestibule once the voltage drops back to -90mV. From Fig. 6(b), the forward moving order of arginines is R1, R2, R3 and R4, and the backward moving order is the opposite R4, R3, R2 and R1 with agreement with the structure. This agreement might look trivial in MD simulations, but is not a trivial check~~ing~~ here since the present model describes arginines not by particles as in MD but by concentrations. Besides, incorrect order and pace of the movement of arginines would cause the disagreement with experiments in the shape of IV curve as well. Note that S4 is initially farthest to the right but lags behind R1 and R2 during movement in depolarization, as shown in Fig. 6(b). This is certainly because S4 is initially relaxed to an almost unforced situation close to its natural position $Z_{S4,0}$. We can further calculate the displacements of each arginine and S4 during this full saturating depolarization, and find $\Delta z_{1,CM} \approx \Delta z_{2,CM} \approx \Delta z_{3,CM} \approx 1.93$nm, $\Delta z_{4,CM}$=1.76nm, ΔZ_{S4}=1.51nm. Besides almost the same displacements for R1, R2 and R3, their average moving velocities are also very close to each other. Near identity in velocity seems to suggest a synchronized movement among R1, R2 and R3 that we have ***not*** (knowingly) imposed on the arginines in our model. Also, we can see the movements of arginines contribute significantly to the movement of the S4 segment**.** This can be seen from the steady state z-position of S4 derived from Eq. (6),

$$Z_{S4} = \frac{K}{K_{S4}+4K}\sum_{i=1}^{4}\left(z_{i,CM} - z_i\right) + \frac{K_{S4}}{K_{S4}+4K}Z_{S4,0} = \frac{1}{5}\left[Z_{S4,0} + \sum_{i=1}^{4} z_{i,CM}\right].$$

Experimental estimates of S4 displacement during full depolarization range from 2-20 Å [15,24] depending on the model of the voltage sensor and its motion. Including the transporter model, the helical screw, and the paddle model [15]. Our ΔZ_{S4}=1.51 nm here is large and seems to agree better with experimental estimates requiring large displacements, such as the paddle model. However, our model was inspired by the helical screw model, which is known to have shorter displacements. A

plausible explanation for our over-estimate of ΔZ_{S4} is that our one-dimensional model uses a straight-line perpendicular to the hydrophobic plug path for the movement of the arginines. In reality, the S4 segment is significantly tilted with respect to the membrane and the arginines follow a spiral along the helix. Therefore if the S4 segment rotates and changes its tilt during activation the total vertical translation needed to cross the hydrophobic plug is significantly reduced, as was shown by Vargas et al [26]. The value obtained in [26] was between 0.7 to 1 nm when comparing the displacement perpendicular to the membrane of the open-relaxed state crystal structure of Kv1.2 [25] and the closed structure that has been derived by consensus from experimental measurements [26].

In the partially depolarized case the driving force is weaker than in a large saturating depolarization, so their *z*-positions do not have a chance to reach steady states as they do during a full saturating depolarization. Rather in a partial depolarization the motion of the arginines and S4 are aborted. They return to the intracellular vestibule because the depolarization drops (i.e., decreases in magnitude) before arginines and S4 have a chance to reach their saturated positions. This detailed atomic interpretation likely over reaches the resolution of our model. We look forward to measurements of movements of probes that mimic arginine ~~and~~ in its environment that require improvements in the resolution and structural realism of our model.

Fig. 6(c) illustrates these aborted motions. *Q* reaches 1.57 at most which should be 2 instead if saturation were reached as it is if time is long enough. See the saturated behavior shown in QV curve of Fig. 2(a). Fig. 6(d) shows that the S4 segment is initially farthest to the right and lags behind R1 during movement and is almost caught up by R2. The maximum displacements of arginines and S4 calculated from Fig. 6(d) are $\Delta z_{1,CM}$ =1.36nm, $\Delta z_{2,CM}$ =0.966nm, $\Delta z_{3,CM}$ =0.459nm, $\Delta z_{4,CM}$ =0.316nm, and $\Delta Z_{4,CM}$ =0.616nm. The significant difference between $\Delta z_{1,CM}$, $\Delta z_{2,CM}$ and $\Delta z_{3,CM}$, $\Delta z_{4,CM}$ may imply that R1 and R2 have jumped across hydrophobic plug and entered extracellular vestibule, while R3 and R4 still stay at intracellular vestibule during this partial depolarization. This is consistent with the observation from individual gating current components of arginines in Fig. 3(d).

Family of gating currents for a range of voltages

Though we prefer $I\left(L_R+\frac{L}{2},t\right)$ to $I(0,t)$ for representing gating current as explained in the section under heading *Flux of charges at different locations*, we here use the actual gating current, de-spiked $I(0,t)$, to compare with experiment [11]. Fig. 7(a) shows the time courses of subtracted gating current (de-spiked $I(0,t)$) for a range of voltages *V*, ranging from -62mV to -8mV. The area under gating current, for

both on and off parts, increases with *V* since more arginines are transferred to extracellular vestibule as *V* increases. The shapes of this family of gating currents agree well with experiment [11] in both magnitude and time course.

We can characterize the time course by fitting the decay part of a subtracted gating current by $ae^{-t/\tau_1} + be^{-t/\tau_2}$, $\tau_1 < \tau_2$, as generally ~~conducted~~ done in experiments [11], where τ_1 is the fast time constant and τ_2 is the slow time constant. Usually the movement of arginines is dominated by τ_2. Here τ_2 was calculated from simulation and compared with experiment [11] as shown in Fig. 7(b). Since in our computation the time is in arbitrary units, we have scaled the time to have the maximum τ_2 to fit with its counterpart in experiment [11]. Overall, the trend of τ_2 versus *V* in our result, though not the whole curve, agrees well with experiment [11]. ~~For the left branches~~To the left of ~~to~~ the maximum point in Fig. 7(b), simulation results fit rather well with experiment compared with the values to the right~~right branches to~~ of ~~the~~ the maximum point, where it overestimates τ_2 compared with experiment. This overestimate is consistent with the observation that the amount of transferred charges *Q* saturates slightly faster in experimental data than in present simulation, as *V* increases (see QV curve of Fig. 2(a)). This phenomenon is related to cooperativity of movement among arginines, that will be further discussed below.

Effect of voltage pulse duration

Fig. 8 shows the effect of voltage pulse duration with Fig. 8(a) for the case of partial depolarization and Fig. 8(b) for the case of full depolarization. Magnitude and time span of subtracted gating current (de-spiked $I(0,t)$) are changed by pulse duration in both cases, but the shape will asymptotically approach the same curve as pulse duration increases, no matter what the size of the depolarization. This behavior occurs because it takes time for the command pulse to drive the arginines towards the extracellular vestibule. If the pulse duration is long enough, the time course of *Q* will approach its steady state for large depolarization, as in Fig. 6(a). Partial depolarization takes longer time to reach its steady state as demonstrated in Fig. 6(c). The shapes of gating currents in Fig. 8 compare favorably with experiment [11], where the OFF subtracted gating currents for short pulses have very fast decays while for long pulses the OFF subtracted gating currents have rising phase and slower decay.

CONCLUSIONS

The present one-dimensional mechanical model of the voltage sensor tries to capture the essential structural details of the movement of mass and charge that are necessary to reproduce the basic features of experimentally recorded gating currents.

After finding appropriate parameters, we find that the general kinetic and steady-state properties are well represented by the simulations. The good agreement of our numerical results with salient features of gating current measured experimentally would be impossible by simply tuning of parameters if our model has not captured the essence of physics for voltage sensor. The continuum approach seems to be a good model of voltage sensors, provided that it i) takes into account all interactions crucial to the movement of gating charges and S4; ii) computes their correlations consistently, so all variables satisfy all equations under all conditions, with one set of parameters, and iii) satisfies conservation of current. This last point gave us a new insight: what is measured experimentally does not correspond to the transfer of the arginines because the total current, containing a displacement current, is smaller than the arginine current.

We have simplified the profile of energy barrier in the hydrophobic plug since the PMF in that region, and its variation with potential and conditions, is unknown. There is plenty of detailed information on the amino acid side chains in the plug and how each one of them changes the kinetics and steady-state properties of gating charge movement [6]. Therefore the next step is to model the details of interactions or the moving arginines with the wall of the hydrophobic plug and the contributions from other surrounding charged protein components. Some of the effects to be included are

1) Steric and dielectric interactions of the arginines that the present model does not include. These interactions may be responsible for the simultaneous movement of two to three arginines across the plug, which is an experimental result that the present model does not reproduce [27,28].
2) Time dependence of the plug energy barrier V_b. Once the first arginine enters the hydrophobic plug by carrying some water with it, this partial wetting of the hydrophobic plug will lower V_b, chiefly consisting of solvation energy, and enable the next arginine to enter the plug with less difficulty. This might explain the cooperativity of movement among arginines when they jump through the plug. The addition of details in the plug may also produce intermediate states that have been measured experimentally. In this situation arginines may transiently dwell within the plug.
3) A very strong electric field might affect the hydration equilibrium of the hydrophobic plug and would lower its hydration energy barrier as well [29]. This cooperativity of movement may help explain the quick saturation in the upper right branch of QV curve (and smaller τ_2). It may also explain the experimentally observed translocation of two to

three arginines simultaneously [27,28].

The power of the present mathematical modeling is precisely the implementation of interactions, and various effects, in a consistent manner. Implementing the various effects listed above is likely to lead to a better prediction of the currents and to the design of experiments to further test and extend the model.

Further work must address the mechanism of coupling between the voltage sensor movements and the conduction pore. It seems likely that the classical mechanical models of coupling will need to be extended to include coupling through the electrical field. The charges involved are large. The distances are small, so the changes in electric forces that accompany movements of mass are likely to be large and important. It is possible that the voltage sensor modifies the stability of a fundamentally stochastically unstable, nearly bistable conduction current by triggering sudden transitions from closed to open state, in a controlled process reminiscent of Coulomb blockade in a noisy environment [30].

已註解 [A1]: This is Bob's comment

It is more polite here to cite some of the work of the Lancaster/Kaufman group. They have done the only specific work on Coulomb blockade in channels (I do not include vague Russian suggestions) although they refused to say much about single channel transisitions no matter how much I suggested that. I do not in fact remember if that idea was ever specifically stated in those papers. It certainly was not emphasized to my horror, so it is understandable if you do not want to cite the work.
Let me know if you want a specific reference.

ACKNOWLEDGMENTS

This research was sponsored in part by NIH grant R01GM030376 (F.B.), MOST (Ministry of Science and Technology of Taiwan) grants MOST-102-2115-M-002-015-MY4 (T.L.H.) and MOST-104-2115-M-035-002-MY2 (T.L.H.). Dr. Horng also thanks the support of National Center for Theoretical Sciences Mathematical Division of Taiwan (NCTS/MATH), and Dr. Ren-Shiang Chen for the long-term helpful discussions.

References (31-42) appear at Supplementary Information.

REFERENCES

[1] Hodgkin, A.L., and A.F. Huxley. 1952. A quantitative description of membrane current and its application to conduction and excitation in nerve. *J. Physiol*. 117:500-544.

[2] Feynman, R.P., R.B. Leighton, and M. Sands. 1963. The Feynman lectures on physics, Vol. 2: mainly electromagnetism and matter. Addison-Wesley, New York.

[3] Jimenez-Morales, D., J. Liang, and B. Eisenberg. 2012. Ionizable side chains at catalytic active sites of enzymes. *Eur. Biophy. J.* 41(5):449-460.

[4] Eisenberg, B., Y.K. Hyon, and C. Liu. 2010. Energy variational analysis EnVarA of ions in water and channels: field theory for primitive models of complex ionic fluids. *J. Chem. Phys.* 133:104104.

[5] Horng, T.L., T.C. Lin, C. Liu, and B. Eisenberg. 2012. PNP equations with steric effects: a model of ion flow through channels. *J. Phys. Chem. B.* 116(37):11422-11441.
[6] Lacroix, J.J., H.C. Hyde, F.V. Campos, and F. Bezanilla. 2014. Moving gating charges through the gating pore in a Kv channel voltage sensor. *Proc. Natl. Acad. Sci. USA.* 111:1950-1959.
[7] Zhu, F., and G. Hummer. 2012. Drying transition in the hydrophobic gate of the GLIC channel blocks ion conduction. *Biophys. J.* 103:219-227.
[8] Schuss, Z., B. Nadler, and B. Eisenberg. 2001. Derivation of Poisson and Nernst-Planck equations in a bath and channel from a molecular model. *Phys. Rev. E.* 64:036116.
[9] Schuss, Z. 2009. Theory And Applications Of Stochastic Processes: An Analytical Approach. Springer, New York.
[10] Lin, T.C., and B. Eisenberg. 2014. A new approach to the Lennard-Jones potential and a new model: PNP-steric equations. *Comm. Math. Sci.* 12(1):149-173.
[11] Bezanilla, F., E. Perozo, and E. Stefani. 1994. Gating of K^+ channels : II. The components of gating currents and a model of channel. *Biophy. J.* 66:1011-1021.
[12] Eisenberg, B. 2016a. Conservation of Current and Conservation of Charge. https://arxiv.org/abs/1609.09175.
[13] Eisenberg, B. 2016b. Maxwell Matters. https://arxiv.org/pdf/1607.06691.
[14] Eisenberg, B., X. Oriols, and D. Ferry. 2017. Dynamics of current, charge, and mass. *Mol. Based Math. Biol*. 5:78-115. https://arxiv.org/abs/1708.07400.
[15] Tombola, F., M.M. Pathak, and E.Y. Isacoff. 2006. How does voltage open an ion channel? *Annu. Rev. Cell Dev. Biol.* 22:23-52.
[16] Bezanilla, F. 2008. How membrane proteins sense voltage. *Nat. Rev. Mol. Cell Biol*. 9:323–332.
[17] Peyser, A. and W. Nonner. 2012, The sliding-helix voltage sensor: mesoscale views of a robust structure–function relationship, *Eur. Biophys. J.* 41:705–721.
[18] Peyser, A. and W. Nonner. 2012, Voltage sensing in ion channels: mesoscale simulations of biological devices, *Phys. Rev. E.* 86:011910.
[19] Schneider, M.F., and W.K. Chandler. 1973. Voltage dependent charge movement in skeletal muscle: a possible step in excitation contraction coupling. *Nature.* 242:244-246.
[20] Bezanilla, F., and C.M. Armstrong. 1975. Properties of the sodium channel gating current. *Cold Spring Harb. Symp. Quant. Biol.* 40: 297-304.
[21] Eisenberg, B. 1996. Computing the field in proteins and channels. *J. Membrane Biol*. 150:1–25. https://arxiv.org/pdf/1009.2857.

[22] Schoppa, N.E., K. McCormack, M.A. Tanouye, and F.J. Sigworth. 1992. The size of gating charge in wild-type and mutant shaker potassium channels. *Science*. 255:1712–1715.

[23] Seoh, S.-A., D. Sigg, D.M. Papazian, and F. Bezanilla. 1996. Voltage-sensing residues in the S2 and S4 segments of the Shaker K+ channel. *Neuron*. 16:1159–1167.

[24] Kim, D.M. and C.M. Nimigean. 2016. Voltage-gated potassium channels: a structural examination of selectivity and gating. *Cold Spring Harb. Perspect. Biol*. 8:a029231.

[25] Chen, X., Q. Wang, F. Ni, and J. Ma. 2010. Structure of the full-length Shaker potassium channel Kv1.2 by normal-mode-based X-ray crystallographic refinement. *Proc. Natl. Acad. Sci. USA.* 107(25):11352-11357.

[26] Vargas, E., F. Bezanilla, and B. Roux. 2011. In search of a consensus model of the resting state of a voltage-sensing domain. *Neuron*. 72(5):713-20.

[27] Conti, F., and W. Stühmer. 1989. Quantal charge redistributions accompanying the structural transitions of sodium channels. *Eur. Biophys. J*. 17:53-59.

[28] Sigg, D., E. Stefani, and F. Bezanilla. 1994. Gating current noise produced by elementary transitions in shaker potassium channels. *Science.* 264:578-582.

[29] Vaitheeswaran, S., J.C. Rasaiah, and G. Hummer. 2004. Electric field and temperature effects on water in the narrow nonpolar pores of carbon nanotubes. *J. Chem. Phys.* 121(16):7955-7965.

[30] Kaufman, I.Kh., P.V.E. McClintock, and R.S. Eisenberg. 2015. Coulomb blockade model of permeation and selectivity in biological ion channels. *New J. Phys.* 17:083021.

[31] Trefethen, L.N. 2000. Spectral Methods in MATLAB. SIAM, Philadelphia.

[32] Ascher, U.M., and L.R. Petzold. 1998. Computer methods for ordinary differential equations and differential-algebraic equations. SIAM, Philadelphia.

[33] Shampine, L.F., and M.W. Reichelt. 1997. The MATLAB ODE Suite. *SIAM J. Sci. Comput*. 18:1–22.

[34] Shampine, L.F., M.W. Reichelt, and J.A. Kierzenka. 1999. Solving Index-1 DAEs in MATLAB and Simulink. *SIAM Rev*. 41:538–552.

[35] Sigg, D., F. Bezanilla, and E. Stefani. 2003. Fast gating in the Shaker K+ channel and the energy landscape of activation. *Proc. Natl. Acad. Sci. USA.* 100:7611-7615.

[36] Stefani, E., and F. Bezanilla. 1997. Voltage dependence of the early events in voltage gating. *Biophys. J.* 72:131.

[37] Stefani, E., D. Sigg, and F. Bezanilla. 2000. Correlation between the early component of gating current and total gating current in Shaker K channels. *Biophys. J.* 78:7.

[38] Forster, I.C., and N.G. Greeff. 1992. The early phase of sodium channel gating current in the squid giant axon. Characteristics of a fast component of displacement charge movement. *Eur. Biophys. J.* 21(2): 99-116.

[39] Armstrong, C.M., and F. Bezanilla. 1974. Charge movement associated with the opening and closing of the activation gates of the sodium channels. *J. Gen. Physiol.* 63:533-552.

[40] Bezanilla, F., and J. Vergara. 1980. Properties of Excitable membranes. *In* Membrane structure and Function. E.E. Bittar, editor. Vol. II, Ch. 2. J. Wiley & Sons, New York, 53-113.

[41] Bezanilla, F., and C.M. Armstrong. 1977. Inactivation of the sodium channel. I. Sodium current experiments. *J. Gen. Physiol.* 70(5):549-566.

[42] Fernández, J.M., F. Bezanilla, and R.E. Taylor. 1982. Distribution and kinetics of membrane dielectric polarization. II. Frequency domain studies of gating currents. *J. Gen. Physiol.* 79(1):41-67.

格式化: 英文 (美國)

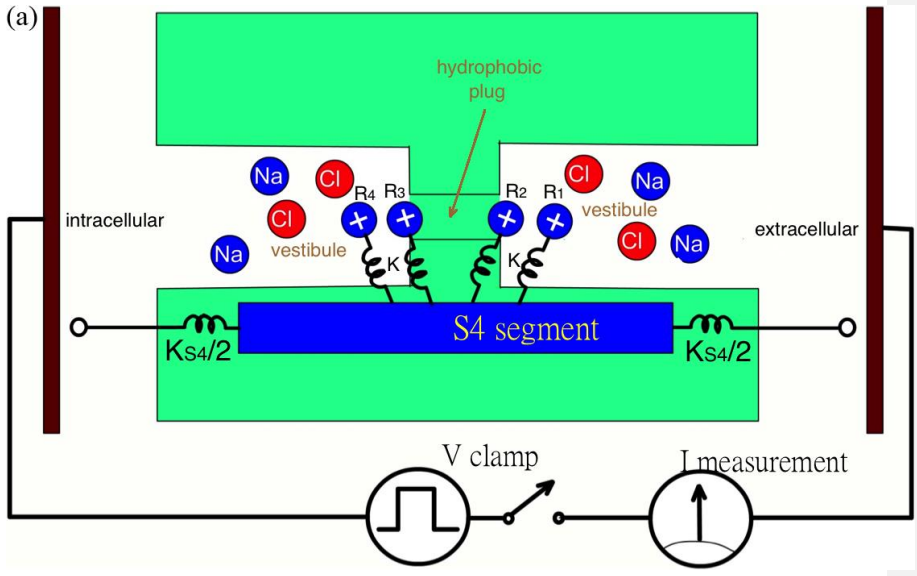

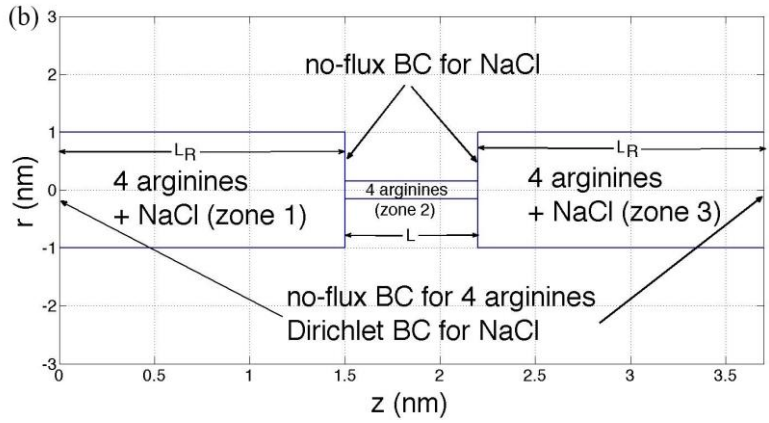

Figure 1. (a) Geometric configuration of gating pore in the present model including the attachments of arginines to the S4 segment. (b) Following (a), an axisymmetric 3-zone domain shape is designated in *r*-*z* coordinate for the current 1D model. Here the diameter of hydrophobic plug is 0.3nm (arginine's diameter); L=0.7nm; L_R=1.5nm; radius of vestibule is R=1nm. BC means Boundary Condition.

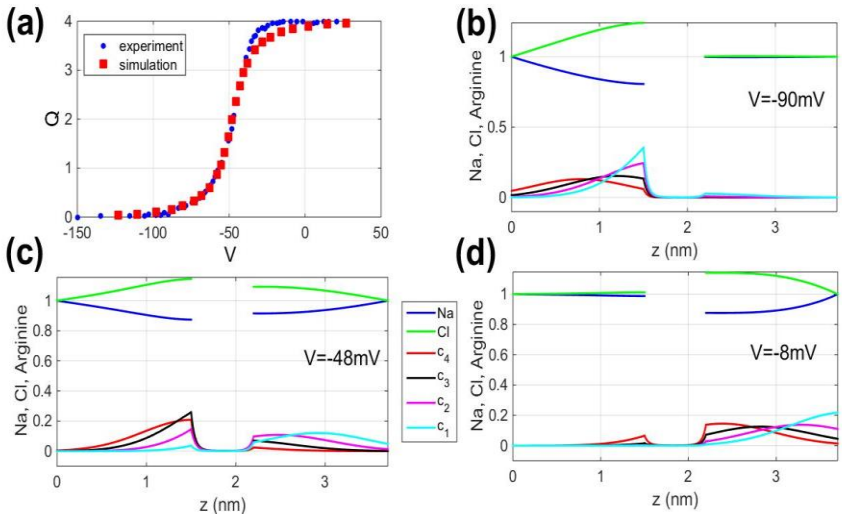

Figure 2. (a) QV curve and comparison with [11]. Steady-state distributions for Na, Cl and arginines at (b) V=-90mV, (c) V=-48mV, (d) V=-8mV.

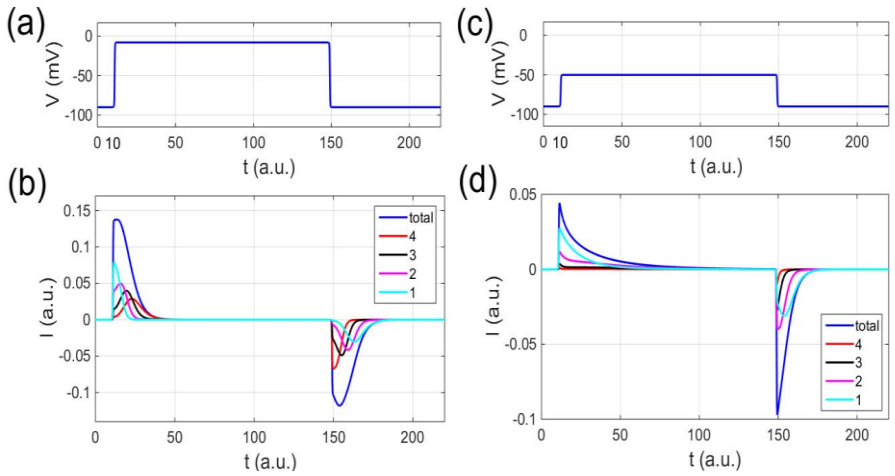

Figure 3. (a) Time course of V rising from -90mV to -8mV at t=10, holds on till t=150, and drops back to -90mV, (b) time course of gating current, $I(L_R + L/2, t)$, and its components corresponding to (a), (c) time course of V rising from -90mV to -50mV at t=10, holds on till t=150, and drops back to -90mV, (d) time course of gating current, $I(L_R + L/2, t)$, and its components corresponding to (c).

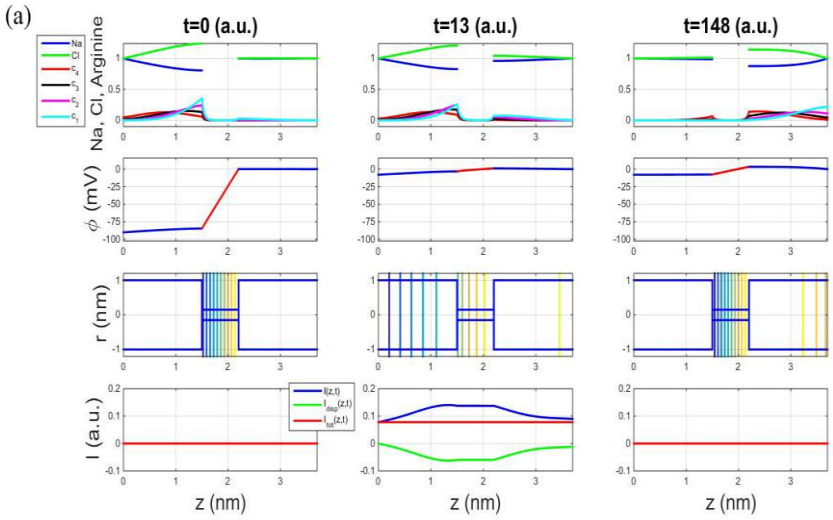

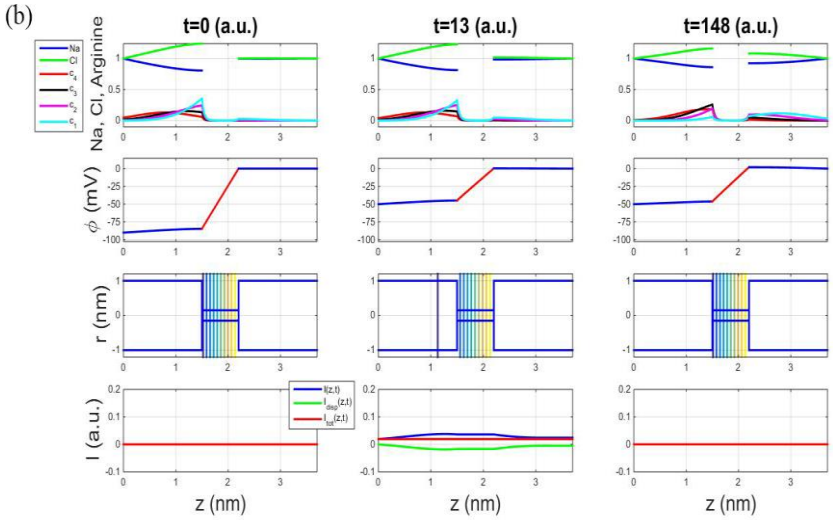

Figure 4. (a) The top row are dimensionless species concentration distributions at t=0, 13, 148, for the case of large depolarization with V from -90mV at t=10 to -8mV, and dropping back to -90mV at t=150. The second row shows concurrent electric potential profiles. The third row show 11 equipotential lines under equal potential increment from smallest to largest potential values at the time indicated superposed on voltage sensor domain as displayed in Figure 1(b). The bottom row shows concurrent electric current profiles with components of flux of charge, displacement current and total current. (b) Same as (a) except with V depolarized from -90mV to -50mV.

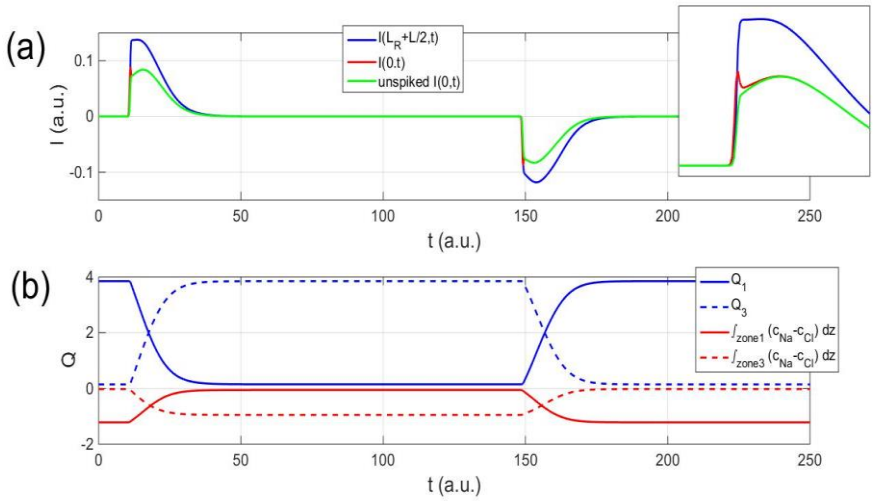

Figure 5. (a) Time courses of $I\left(L_R+\frac{L}{2},t\right)$, $I(0,t)$ and de-spiked $I(0,t)$ for the case of full depolarization with V rising from -90mV to -8mV at t=10, holding on till t=150, and dropping back to -90mV. The inset plot is a magnification of ON-current to visualize the difference of $I(0,t)$ and de-spiked $I(0,t)$ more clearly. (b) Time courses of $Q_1, Q_3, \int_0^{L_R}(c_{Na}-c_{Cl})\,dz$, and $\int_{L_R+L}^{2L_R+L}(c_{Na}-c_{Cl})\,dz$ under the same depolarization scenario as (a).

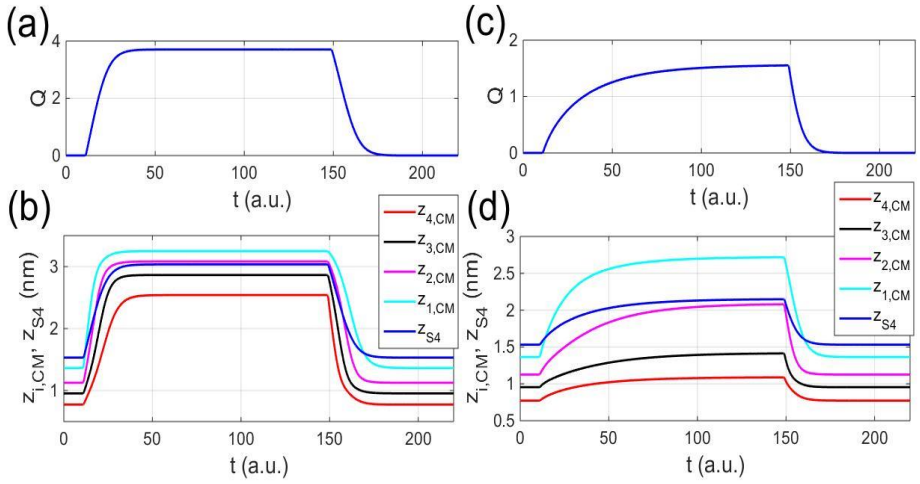

Figure 6. (a) and (c) are time courses of amount of arginines moved to extracellular vestibule. (b) and (d) are center-of-mass trajectories of individual arginines and S4. (a) and (b) are the case of large depolarization with V rising from -90mV to -8mV at t=10, holding on till t=150, and dropping back to -90mV. (c) and (d) are the case of partial depolarization with V rising from -90mV to -50mV at t=10, holding on till t=150, and dropping back to -90mV.

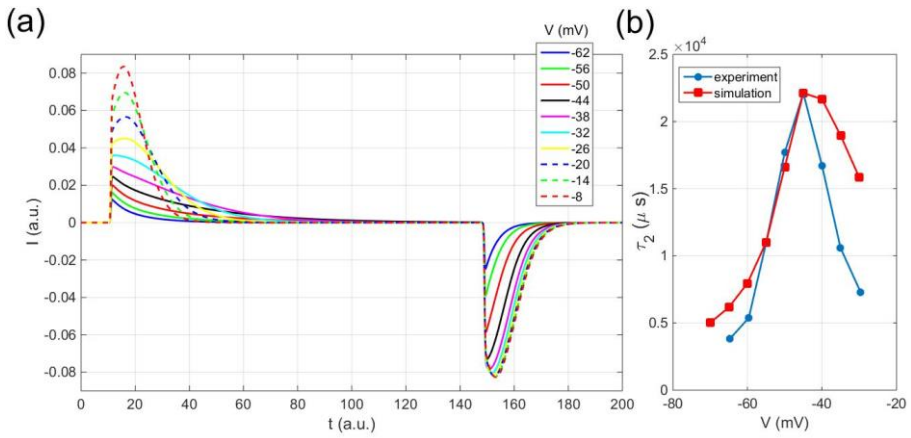

Figure 7. (a) Time courses of subtracted gating current, de-spiked $I(0,t)$, with voltage rising from -90mV to VmV at t=10, holds on till t=150, and drops back to -90mV, where V=-62, -50, … -8 mV. (b) τ_2 versus V compared with experiment [11].

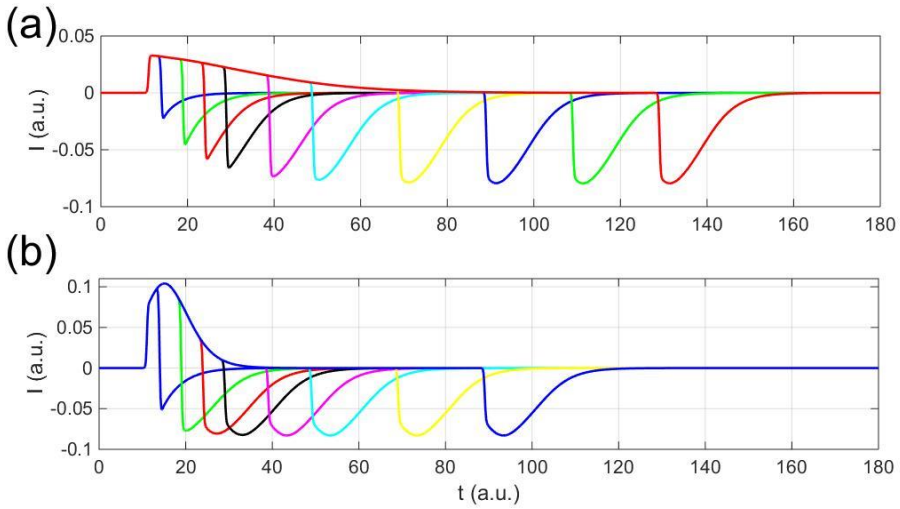

Figure 8. Subtracted gating currents, de-spiked $I(0,t)$, showing effect of voltage pulse duration: (a) V increases from -90mV to -35mV at t=10 and drops back to -90mV at various times, (b) V increases from -90mV to 0mV at t=10 and drops back to -90mV at various times.

SUPPLEMENTARY INFORMATION

Continuum Gating Current Models Computed with Consistent Interactions
Tzyy-Leng Horng , Robert S. Eisenberg, Chun Liu, Francisco Bezanilla

1. Non-dimensionalization

We non-dimensionalize all physical quantities as follows,

$\tilde{c}_i = \frac{c_i}{c_0},\ \tilde{\phi} = \frac{\phi}{k_BT/e}, \tilde{U} = \frac{U}{k_BT},\ \tilde{s} = \frac{s}{R},\ \tilde{t} = \frac{t}{R^2/D_x},\ \tilde{D}_i = \frac{D_i}{D_x},\ \tilde{g}_{ij} = \frac{g_{ij}}{k_BT/c_0},\ \tilde{J}_i = \frac{J_i}{c_0D_xR/R},$

$\tilde{I} = \frac{I}{ec_0D_xR},$

where c_i is concentration of species *i*, with *i*=Na^+, Cl^-, 1, 2, 3, and 4. Each is scaled by c_0 which is the bulk concentration of NaCl at the intracellular/extracellular domains. Here c_0 is set to be 184 mM, equal on both sides, so that the Debye length $\lambda_D = \sqrt{\frac{\varepsilon_r\varepsilon_0k_BT}{c_0e^2}}$ is 1nm when the relative permittivity $\varepsilon_r = 80$. Note that the concentrations c_i, *i*=1, 2, 3, and 4 need to satisfy the following additional constraint $\int_0^{L+2LR} A(z)c_i dz = 1$ due to uniqueness of each arginine, with $A(z)$ being the cross-sectional area of channel shown in Fig. 1(b) at position *z*. ϕ is the electric potential scaled by k_BT/e with k_B being the Boltzmann constant; T the temperature; *e* the elementary charge. All relevant external potentials *U* are scaled by k_BT. All sizes *s* are scaled by *R*, which is the radius of vestibule as shown in Fig. 1(b). *R*=1nm here. The time *t* is scaled by R^2/D_x, with D_x being a diffusion coefficient that can be adjusted later to be consistent with the time spans of on/off currents measured in experiments (caused by the movement of arginines). The diffusion coefficient of species *i* is scaled by D_x. The coupling constant g_{ij} of PNP-steric model based on combining rules of Lennard Jones, representing the strength of steric interaction between species *i* and *j*, is scaled by k_BT/c_0 [1,2]. For simplicity, we assume $g_{ij} = \begin{cases} g, & \text{for all } i \neq j \\ 0, & \text{for all } i = j \end{cases}$, $i,j = 1,2,3,4$. Note that here we only consider steric interaction among arginines. We think they are a crucial source of correlated structural change and motion (of mass and charge). The consideration of steric effect among arginines is justified by the fact that arginines are generally crowded in hydrophobic plug and vestibules. The flux density of species *i*, J_i, is scaled by c_0D_x/R, and therefore the electric current *I* is scaled by ec_0D_xR. For simplicity of notation, we will drop ~ for all dimensionless quantities shown in all equations.

2. Shape of potential of mean force (PMF) in the hydrophobic plug

Here, we simply assume a hump shape for PMF in the hydrophobic plug as,

$$\begin{cases} V_b = V_{b,max}\left(\tanh\left(5(z-L_R)\right) - \tanh\left(5(z-L-L_R)\right) - 1\right), & when\ z \text{ is in zone 2,} \\ V_b = 0, & when\ z \text{ is in zone 1 and 3,} \end{cases} \quad \text{(S1)}$$

with $V_{b,max}$ set to be 5 for a good agreement with experimental measurements. Theoretically, if we set $V_{b,max}$ too large, the gating current would be slow and perhaps small because it would be very difficult for arginines to move across this barrier. The double *tanh* functions are designed to smooth the otherwise top-hat-shape barrier profile, which is not good for numerical differentiation because of its awkward infinite slopes. This smoothing is simply based on the belief that the energy barrier in a protein structure does not have a jump. In future work, it would be wise to compute the PMF from a specific model of charge distribution (both permanent and polarization) constructed from a combination of structural data and molecular dynamics simulations, if feasible.

已註解 [A2]: I hope you all agree and the wording is OK. I left out the lumped capacitor representation as too likely to show our hand to competitors.

3. Governing equations derivation from energy variation methods

Governing equations Eqs. (1-4) were derived by energy variational methods based on the following energy (in dimensional form):

$$E = \int_V \left[k_B T \sum_{all\ i} c_i log c_i - \frac{\varepsilon_0 \varepsilon_r}{2}|\nabla\phi|^2 + \sum_{all\ i} z_i e\, c_i \phi + \sum_{arginines}(V_i + V_b)\, c_i + \sum_{arginines\ i,j} \frac{g_{ij}}{2} c_i c_j\right] dV, \quad \text{(S.2)}$$

where the first term is entropy; second and third terms are electrostatic energy; the fourth term is the constraint and barrier potential for arginines; the last term is the steric energy term, based on Lennard-Jones potential [1,3]. The Poisson equation Eq. (1) is derived from the variation of energy with respect to electric potential

$$\frac{\delta E}{\delta \phi} = 0,$$

and species flux densities in Eqs. (3,4) are derived by

$$\mu_i = \frac{\delta E}{\delta c_i}, \qquad J_i = -\frac{D_i}{k_B T} c_i \nabla \mu_i,$$

where μ_i is the chemical potential of species i.

4. Quasi-steadiness assumption for Na^+ and Cl^-

Here we assume quasi-steady state for Na^+ and Cl^-, which means $\frac{\partial c_i}{\partial t} = 0, i = Na, \mathrm{Cl}$. The steady state assumption here is justified by the fact that the diffusion coefficients of Na^+ and Cl^- in vestibules are much larger than the diffusion coefficient of arginine based on the very narrow time span of the leading spike of gating current measured in experiments. The spike comes from the linear capacitive current of vestibule when the command potential suddenly rises or drops. This quasi-steady state assumption is essential for the success of our calculations. Otherwise using realistic diffusion coefficients for Na^+ and Cl^- would render Eqs. (1-4) too stiff to integrate in time. The spike contaminating the gating current is removed in experiments by a simple technique called ***P/n*** leak subtraction (see Section 11). ***P/n*** leak subtraction is also used to subtract the linear capacity current of all the membranes in the real system that are not included in our model. How to do leak subtraction computationally will be discussed in Section 10.

5. Formulation of boundary conditions

Types of boundary conditions is illustrated in Fig. 1(b). Note the no-flux boundary conditions specified in Fig. 1(b). One prevents Na^+ and Cl^- from entering the hydrophobic plug (zone 2) with low dielectric coefficient. The other boundary condition constrains S4 motion and so prevents the arginines from leaving the vestibules into intracellular/extracellular domains.

Boundary and interface conditions for electric potential ϕ are

$$\phi(0) = V, \quad \phi(L_R^-) = \phi(L_R^+), \quad \Gamma(L_R^-)A(L_R^-)\frac{d\phi}{dz}(L_R^-) = \Gamma(L_R^+)A(L_R^+)\frac{d\phi}{dz}(L_R^+),$$
$$\phi(L_R + L^-) = \phi(L_R + L^+), \quad \Gamma(L_R + L^-)A(L_R + L^-)\frac{d\phi}{dz}(L_R + L^-) = \Gamma(L_R + L^+)A(L_R + L^+)\frac{d\phi}{dz}(L_R + L^+), \quad \phi(2L_R + L) = 0. \tag{S.3}$$

These are Dirichlet boundary conditions at both ends and continuity of electric potential and displacement at the interfaces between zones. Boundary and interface conditions for arginine are

$$J_i(0,t) = J_i(2L_R + L, t) = 0, \; c_i(L_R^+, t) = c_i(L_R^-, t), \quad A(L_R^-)J_i(L_R^-, t) = A(L_R^+)J_i(L_R^+, t), \; c_i(L_R + L^-, t) = c_i(L_R + L^+, t), \; A(L_R + L^-)J_i(L_R + L^-, t) = A(L_R + L^+)J_i(L_R + L^+, t), \; i = 1,2,3,4, \tag{S.4}$$

where no-flux boundary conditions are placed at both ends of the gating pore, consisting of vestibules and hydrophobic plug, to prevent arginines and S4 from entering intracellular/extracellular domains. The others are continuity of concentration and flux at interfaces between zones. Boundary conditions for Na^+ and Cl^- are

$$c_{Na}(0,t) = c_{Cl}(0,t) = c_{Na}(2L_R + L, t) = c_{Cl}(2L_R + L, t) = 1,$$
$$J_{Na}(L_R, t) = J_{Cl}(L_R, t) = J_{Na}(L_R + L, t) = J_{Cl}(L_R + L, t) = 0, \quad \text{(S.5)}$$

where Dirichlet boundary conditions are placed at both ends of the gating pore to describe the concentrations for Na^+ and Cl^- as the bulk concentration. No-flux boundary conditions at both ends of hydrophobic plug describe the impermeability of Na^+ and Cl^- into hydrophobic plug.

6. Parameters fitting

We have tried and found D_i=50, i=1,2,3,4, K=3, K_{S4}=3, b_{S4}=1.5 provide the best fit to the important experiments reported in [4]. Several things are to be noted about the parameter values specified above: (1) there is no experimental measurement of diffusion coefficient of arginine inside vestibule and plug available that we can use for simulation. Imprecise setting of these diffusion coefficient values only affects the scale of time in I-V curve, but not its shape. That is why we set time coordinate to be in an arbitrary unit later in results, and here we only focus on comparing the shape of IV curves with experiments in [4]. (2) K, K_{S4}, and b_{S4} were particularly determined by fitting with QV curve in experiment [4]. QV curve is very sensitive to K, K_{S4}, and b_{S4}, and many efforts have been taken to achieve these values.

7. Derivation of Ampere's law in Maxwell's equations by Poisson equation and species transport equation

Eq. (8) is consistent with Ampere's law in Maxwell's equations:

$$\nabla \times \left(\frac{\vec{B}}{\mu_0}\right) = \varepsilon_0 \varepsilon_r \frac{\partial \vec{E}}{\partial t} + \vec{J}, \quad \text{(S.6)}$$

or equivalently,

$$\nabla \cdot \left(\varepsilon_0 \varepsilon_r \frac{\partial \vec{E}}{\partial t} + \vec{J}\right) = 0, \quad \text{(S.7)}$$

where $\vec{E}$ is the electric field and $\vec{J}$ is flux density of charge (current density). Eq. (S.7) tells us that the total current is conserved everywhere and it consists of flux of charges $\vec{J}$ and displacement current $\varepsilon_0 \varepsilon_r \frac{\partial \vec{E}}{\partial t}$. Eq. (S.7) can be derived from the Poisson equation and species transport equation like Eq. (1) and Eq. (2). Starting from Poisson equation in dimensional form:

$$-\nabla \cdot (\varepsilon_0 \varepsilon_r \nabla \phi) = \rho + \sum_i z_i e c_i, \quad \text{(S.8)}$$

or equivalently

$$\nabla \cdot \left(\varepsilon_0 \varepsilon_r \vec{E}\right) = \rho + \sum_i z_i e c_i. \quad \text{(S.9)}$$

Taking time derivative of Eq. (S.9),

$$\nabla \cdot \left(\varepsilon_0 \varepsilon_r \frac{\partial \vec{E}}{\partial t}\right) = \sum_i z_i e \frac{\partial c_i}{\partial t}, \qquad \text{(S.10)}$$

and using species transport equation based on mass conservation,

$$\frac{\partial c_i}{\partial t} + \nabla \cdot \vec{J}_i = 0, \qquad \text{(S.11)}$$

then

$$\nabla \cdot \left(\varepsilon_0 \varepsilon_r \frac{\partial \vec{E}}{\partial t}\right) = \sum_i z_i e \frac{\partial c_i}{\partial t} = -\nabla \cdot \sum_i z_i e \vec{J}_i = -\nabla \cdot \vec{J}, \qquad \text{(S.12)}$$

which becomes exactly Eq. (S.7) by defining

$$\vec{J} = \sum_i z_i e \vec{J}_i. \qquad \text{(S.13)}$$

A more general treatment that does not involve assumptions about ε_r can be found in Eisenberg [5-7].

Casting Eq. (S.7) into the present 1D framework by integrating it in space and applying the divergence theorem, we have

$$\varepsilon_0 \varepsilon_r A(z) \frac{\partial E(z,t)}{\partial t} + I(z,t) = \varepsilon_0 \varepsilon_r A(0) \frac{\partial E(0,t)}{\partial t} + I(0,t). \qquad \text{(S.14)}$$

Comparing with Eq. (11),

$$\varepsilon_0 \varepsilon_r A(z) \frac{\partial E(z,t)}{\partial t} - \varepsilon_0 \varepsilon_r A(0) \frac{\partial E(0,t)}{\partial t} = I_{disp}(z,t), \qquad \text{(S.15)}$$

which justifies the naming of displacement current in Eq. (11).

8. Numerical method

High-order multi-block Chebyshev pseudospectral methods are used here to discretize Eqs. (1-4) in space [8]. The resultant semi discrete system is then a set of coupled ordinary differential equations in time and algebraic equations (an ODAE system) [9]. The ordinary differential equations are chiefly from Eq. (2), and algebraic equations are chiefly from Eq. (1) and boundary/interface conditions Eqs. (S.3-S.5). This system is further integrated in time by an ODAE solver (ODE15S in MATLAB [10,11]) together with appropriate initial condition. ODE15S is a variable order variable step (VSVO) solver, which is highly efficient in time integration because it adjusts the time step and order of integration. High-order pseudospectral methods generally provide excellent spatial accuracy with economically practicable resolutions. A combination of these two techniques makes the whole computation very efficient. This is particularly important here, since numerous computations have to be tried during the tuning of parameters. Efficiency will be vital in future calculations comparing theory and experiment in a wide variety of mutants and experimental conditions.

9. Computation of flux of charge, displacement current and total current

According to definition in Eq. (10), flux of charges at the middle of gating pore, $I(L_R + L/2, t)$, and both ends of gating pore, $I(0,t)$ and $I(2L_R + L, t)$, should be computed by

$$I\left(L_R + \frac{L}{2}, t\right) = A\left(L_R + \frac{L}{2}\right)\sum_{arginines} z_i J_i\left(L_R + \frac{L}{2}, t\right), \quad \text{(S.16)}$$

$$I(0,t) = A(0)\sum_{i=Na,Cl} z_i J_i(0,t), \quad \text{(S.17)}$$

$$I(2L_R + L, t) = A(2L_R + L)\sum_{i=Na,Cl} z_i J_i(2L_R + L, t). \quad \text{(S.18)}$$

Except $I\left(L_R + \frac{L}{2}, t\right)$, $I(0,t)$ and $I(2L_R + L, t)$ are trivially zero due to the implement of quasi-steadiness $\frac{\partial c_i}{\partial t} = 0, i = Na, \mathrm{Cl}$, in vestibules, which causes J_{Na} and J_{Cl} to be uniform in vestibules by Eq. (2), and further become zero by the no-flux boundary conditions for Na^+ and Cl^- at the bottom of vestibules as described in Eq. (S.5). We have to alternatively reconstruct $I(0,t)$ and $I(2L_R + L, t)$ by charge conservation of Na^+ and Cl^-,

$$I(0,t) = \frac{d}{dt}\int_0^L A(z)\sum_{Na,Cl} z_i c_i dz, \quad \text{(S.19)}$$

$$I(2L_R + L, t) = -\frac{d}{dt}\int_{L+L_R}^{L+2L_R} A(z)\sum_{Na,Cl} z_i c_i dz. \quad \text{(S.20)}$$

After obtaining $I(0,t)$ and $I(2L_R + L, t)$, we can further reconstruct the flux of charges $I(z,t)$ at zone 1 and zone 3 by charge conservation of Na^+ and Cl^- again,

$$I(z,t) = I(0,t) - \frac{d}{dt}\int_0^z A(z)\sum_{Na,Cl} z_i c_i dz\,, \quad z \in [0, L_R], \quad \text{(S.21)}$$

$$I(z,t) = I(2L_R + L, t) + \frac{d}{dt}\int_z^{2L_R+L} A(z)\sum_{Na,Cl} z_i c_i dz\,, \quad z \in [L_R + L, 2L_R + L]. \quad \text{(S.22)}$$

Once the flux of charges is analyzed, we can then compute the displacement current based on finding the time derivative of Eq. (9), and the summation of flux of charge and displacement current would be the total current.

10. Removing spike in total current

In voltage-clamp experiments, subtracting this linear capacitive component and removing the spike from gating current is done by 'leak subtraction', in various forms, e.g., P/4 (see details in Section 11) In reality, this linear capacitive current that is subtracted in this procedure comes from both the lipid bilayer membrane in parallel with the gating pore. Here, we only considered the capacitive current from solution EDL of vestibule inside the gating pore and ignored the membrane capacitive current

because we simply use Dirichlet boundary conditions for ϕ at both ends of the gating pore in Eq. (S.3). Actually, capacitive current of the membrane in parallel with the gating pore would be much larger than vestibule capacitive current. Following the idea of the experiment [4], we calculated $I(0,t)$ with V rising from -150mV to -140mV at t=10, and dropping back to -150mV at t=150. We chose from -150mV to -140mV because essentially none of the arginines move across the hydrophobic plug in this hyperpolarized region. The voltage step quickly charges and discharges solution EDL in vestibules, and the computed time course of $I(0,t)$ is just two spikes at on and off of the command potential. Subtracting this hyperpolarized $I(0,t)$, multiplied by a proportion factor (due to the linearity of capacitive current), from its original counterpart will then remove the spikes, and the unspiked $I(0,t)$ is shown in Fig. 5(a). In preliminary calculations with the model, when the command voltage pulse rises faster, the early spike becomes larger and is still visible even after subtraction, suggesting that is the origin of the early transient gating current in experiments [12-14].

11. Removing linear capacitive current to obtain gating current in experiments

Our computations have limited fidelity at short times because of time step limitations in integrating stiff systems. The spike artifacts are one example, described previously. Experimental measurements [12,15] of the fast transient gating current are fascinating and our calculations will be extended to explore more of them in future study by using great~~high~~er resolution in time.

A more general consideration is the subtraction procedure used in experiments to isolate gating current from currents arising from other sources. Channels and their voltage sensors are embedded in lipid membranes, therefore they are 'in parallel' with large capacitive currents of the lipid bilayer. The lipid membrane has a large capacitance ($C_{lipid} \cong 8 \times 10^{-7}$ farads/cm^2) that has nothing to do with the current produced by charge movement in the voltage sensor. Fortunately, the capacitance C_{lipid} is a nearly ideal circuit element and the current to charge it is entirely a displacement current accurately described by $i_{cap} = C_{lipid}\,\partial \mathrm{V}/\partial \mathrm{t}$ with a single constant C_{lipid}. V is the voltage across the lipid capacitor. Note that i_{cap} does not include any current or flux of charge carried across the lipid.

In experimental measurements, i_{cap} is always present. Experimental measurements always mix the displacement currents of lipid membrane and voltage sensor. Lipid membrane current usually dominates the measurement of gating currents in native preparations and remains large in systems mutated to have unnaturally large numbers of voltage sensors.

A procedure to remove the lipid membrane current is needed if the gating current of the voltage sensor is to be measured. The procedure introduced by [16] has been

used ever since in the improved P/4 version developed by [17] reviewed and discussed in [18]. Also, see another approach in [19] and [20]. Schneider and Chandler's procedure [19] estimates the so-called linear current $i_x = C_x\,\partial \mathrm{V}/\partial \mathrm{t}$ in conditions in which the voltage sensor and C_x behave as ideal circuit elements. An ideal capacitor has a capacitance C_x independent of voltage, time, current, or ionic composition. The Schneider procedure then subtracts that linear current i_x from the total current measured in conditions in which the voltage sensor does not behave as an ideal capacitor. The leftover estimates the nonlinear properties of the charge movement in the voltage sensor. That is to say, the leftover estimates the charge movement of the voltage sensor that is ***not*** proportional to the size of the voltage step used in the measurement. The leftover is called gating current here and in experimental papers.

The gating current reported in experiments is missing a component of the displacement current of the voltage sensor, if it uses the linear subtraction to estimate i_x. These procedures remove more than the current through the lipid membrane capacitor i_{cap}. Rather, these procedures produce current estimates that contain the lipid membrane current i_{cap} plus current through any structures in the membrane ('in parallel') in which current follows the law $i_x = C_x\,\partial \mathrm{V}/\partial \mathrm{t}$.

Clearly, some of the current produced by movements of the arginines in the voltage sensor will be a linear displacement current, a linear component of gating current and it would not be present in the reported gating current determined by any of the linear subtraction procedures. Other systems may contribute to the linear displacement current as well, for example, i) all sorts of experimental and instrumentation artifacts and ii) displacement current in the conduction channel itself. The conduction channel of field effect transistors produces a large displacement current often characterized as a capacitance that involves diffusion and is described by drift diffusion equations quite similar to the PNP equations of the open conduction channel.

Because our procedure subtracts a hyperpolarized current with arginines that do not move at that voltage, then it removes all the currents carried by arginine movement linear in voltage. Most systems have substantial motions that are linear in voltage (even if the system is labeled 'nonlinear'). The linear term is present in most systems, just as it is present in most Taylor expansions of nonlinear functions.

The linear component missed in experiments, and removed in these calculations, may have functional and structural significance. The voltage sensor works by sensing voltage, for example, by producing a motion of arginines. That motion—the response of the voltage sensor in this model—includes a linear component. The signal passed to the conduction channel, to control gating, is likely to include or depend on the linear component of sensor function. Confusion will result if

a significant linear component exists and is ignored when a model is created that links the voltage sensor to the gating process of the conduction channel. Direct measurements of the movement of arginines (e.g., with optical methods) are likely to include the linear component and so should ***not*** agree with experimental measurements of gating current or with the currents reported here if the linear component exists and is significant in size.

REFERENCES

[1] Horng, T.L., T.C. Lin, C. Liu, and B. Eisenberg. 2012. PNP equations with steric effects: a model of ion flow through channels. *J. Phys. Chem. B.* 116(37):11422-11441.

[2] Lin, T.C., and B. Eisenberg. 2014. A new approach to the Lennard-Jones potential and a new model: PNP-steric equations. *Comm. Math. Sci.* 12(1):149-173.

[3] Eisenberg, B., Y.K. Hyon, and C. Liu. 2010. Energy variational analysis EnVarA of ions in water and channels: field theory for primitive models of complex ionic fluids. *J. Chem. Phys.* 133:104104.

[4] Bezanilla, F., E. Perozo, and E. Stefani. 1994. Gating of K^+ channels : II. The components of gating currents and a model of channel. *Biophy. J.* 66:1011-1021.

[5] Eisenberg, B. 2016a. Conservation of Current and Conservation of Charge. https://arxiv.org/abs/1609.09175.

[6] Eisenberg, B. 2016b. Maxwell Matters. https://arxiv.org/pdf/1607.06691.

[7] Eisenberg, B., X. Oriols, and D. Ferry. 2017. Dynamics of current, charge, and mass. *Mol. Based Math. Biol*. 5:78-115. https://arxiv.org/abs/1708.07400.

[8] Trefethen, L.N. 2000. Spectral Methods in MATLAB. SIAM, Philadelphia.

[9] Ascher, U.M., and L.R. Petzold. 1998. Computer methods for ordinary differential equations and differential-algebraic equations. SIAM, Philadelphia.

[10] Shampine, L.F., and M.W. Reichelt. 1997. The MATLAB ODE Suite. *SIAM J. Sci. Comput*. 18:1–22.

[11] Shampine, L.F., M.W. Reichelt, and J.A. Kierzenka. 1999. Solving Index-1 DAEs in MATLAB and Simulink. *SIAM Rev*. 41:538–552.

[12] Sigg, D., F. Bezanilla, and E. Stefani. 2003. Fast gating in the Shaker K+ channel and the energy landscape of activation. *Proc. Natl. Acad. Sci. USA.* 100:7611-7615.

[13] Stefani, E., and F. Bezanilla. 1997. Voltage dependence of the early events in voltage gating. *Biophys. J.* 72:131.

[14] Stefani, E., D. Sigg, and F. Bezanilla. 2000. Correlation between the early component of gating current and total gating current in Shaker K channels. *Biophys. J.* 78:7.

[15] Forster, I.C., and N.G. Greeff. 1992. The early phase of sodium channel gating current in the squid giant axon. Characteristics of a fast component of displacement charge movement. *Eur. Biophys. J.* 21(2): 99-116.
[16] Schneider, M.F., and W.K. Chandler. 1973. Voltage dependent charge movement in skeletal muscle: a possible step in excitation contraction coupling. *Nature.* 242:244-246.
[17] Armstrong, C.M., and F. Bezanilla. 1974. Charge movement associated with the opening and closing of the activation gates of the sodium channels. *J. Gen. Physiol.* 63:533-552.
[18] Bezanilla, F., and J. Vergara. 1980. Properties of Excitable membranes. *In* Membrane structure and Function. E.E. Bittar, editor. Vol. II, Ch. 2. J. Wiley & Sons, New York, 53-113.
[19] Bezanilla, F., and C.M. Armstrong. 1977. Inactivation of the sodium channel. I. Sodium current experiments. *J. Gen. Physiol.* 70(5):549-566.
[20] Fernández, J.M., F. Bezanilla, and R.E. Taylor. 1982. Distribution and kinetics of membrane dielectric polarization. II. Frequency domain studies of gating currents. *J. Gen. Physiol.* 79(1):41-67.

格式化: 英文 (美國)